Pergamon

Solid-State Electronics Vol. 42, No. 7–8, pp. 1355–1359, 1998

Printed in Great Britain

PII: S0038-1101(98)00030-6

0038-1101/98 $19.00 + 0.00

A FUNCTIONAL CELL FOR QUANTUM-DOT CELLULAR AUTOMATA

G. L. SNIDER, A. O. ORLOV, I. AMLANI, G. H. BERNSTEIN, C. S. LENT, J. L. MERZ and W. POROD

Department of Electrical Engineering, University of Notre Dame, Notre Dame, IN 46556, U.S.A.

Abstract—We present experimental demonstration of a basic cell of Quantum-dot Cellular Automata, a transistorless computation paradigm which addresses the issues of device density and interconnection. The devices presented consist of four and six-dot quantum-dot cellular systems where the metal dots are connected by capacitors and tunnel junctions. The operation of a basic cell is confirmed by the externally controlled polarization change of the cell. The cell exhibits a bistable response and voltage gain. We present an experimental technique which cancels the parasitic cross-talk capacitors in the system. © 1998 Elsevier Science Ltd. All rights reserved

1. INTRODUCTION

Growth in the microelectronics industry is based on a continuing increase in the number of devices fabricated on a chip. For more than 30 years this trend has obeyed Moore's law which predicts that the number of devices integrated on a chip will double every 18–24 months. Adherence to this exponential growth curve has been a monumental task requiring dramatic and rapid improvements in all aspects of integrated circuit (IC) fabrication, where manufacturers both reduced the size of devices and increased chip size while maintaining acceptable yields. One thing that has not changed is the basic device used in the circuits. Since the early 1970s the device of choice for high levels of integration has been the field effect transistor (FET), and while the FET of today is a vast improvement over that of 1970, it is still a FET. At gate lengths below 0.1 μm FETs will begin to encounter fundamental effects which make further scaling difficult. A possible method for the microelectronics industry to maintain continued growth in device density is to change from the FET-based paradigm to one based on nanostructures. Here, instead of fighting the effects that come with feature size reduction, these effects are used to advantage. One nanostructure paradigm, proposed by Lent *et al.*,[1,2] is Quantum-Dot Cellular Automata (QCA), which employs arrays of coupled quantum dots to implement Boolean logic functions[3,4]. The advantage of QCA lies in (1) the extremely high packing densities possible due to the small size of the dots, (2) the simplified interconnection, and (3) the extremely low power-delay product which can be arbitrarily reduced by adiabatic switching[5]. Using QCA cells with dots of 20 nm diameter, an entire full adder can be placed within 1 μm^2, approximately the area of a single 0.07 μm gate length FET.

A basic QCA cell consists of four quantum dots located at the corners of a square, coupled by tunnel barriers. If the cell is biased so that there are two excess electrons among the four dots, Coulomb repulsion will force the electrons to opposite corners. There are thus two energetically equivalent polarizations as shown in Fig. 1(a). These two polarizations can be labeled logic '0' and '1', and by properly arranging cells so that the polarization of one cell sets the polarization of a nearby cell, it is possible to implement all combinational logic functions. A tremendous advantage of QCA devices is the simplified interconnect which is possible with this paradigm. Since the cells communicate only with their nearest neighbors, there is no need for long interconnect lines. The inputs are applied to the cells at the edge of the system and the computation proceeds until the output appears at cells at the edge of the QCA array.

2. EXPERIMENT

The experimental work presented is based on a QCA cell using aluminum islands with aluminum-oxide tunnel junctions, fabricated on an oxidized silicon wafer. The fabrication used standard electron beam lithography and shadow evaporation to form the islands and tunnel junctions[6]. The area of the tunnel junctions is an important quantity since this dominates island capacitance, determining the charging energy of the island and hence the operating temperature of the device. For our devices the area is approximately 60 by 60 nm, giving a junction capacitance of 400 aF.

We recently demonstrated the first step in the development of QCA systems, i.e., a functional QCA cell where we can switch the polarization of a cell, confirming that the switching of a single electron between coupled quantum dots can control the

position of a single electron in another set of dots[7]. A schematic diagram of our four-dot system is shown in Fig. 1(b). The input voltages V_A and V_B are connected to Dots D1 and D2, which are individual dots. These are connected capacitively to the double-dot D3 and D4, which are joined by a tunnel junction. The circuit was mounted on the cold finger of a dilution refrigerator which has a base temperature of 7 mK. The conductance through the double-dot (D3 and D4) and each individual dot D1 and D2 were measured simultaneously using standard ac lock-in techniques with an excitation voltage of 4 μV and a frequency of 16 to 40 Hz. A magnetic field of 1 T was applied to suppress the superconductivity of the aluminum metal. The capacitances between the gates and islands was extracted from the period of the Coulomb blockade oscillations seen in a current–voltage measurement[8].

The operation of a QCA cell is best understood by examining the conductance through the double-dot as a function of the two gate voltages V_C and V_D, as shown in the contour plot of Fig. 2. A peak in the conductance is observed each time the Coulomb blockade is lifted for the double-dot system, and due to the capacitive coupling between the dots, each peak splits into a double peak. The peaks form the vertices of a hexagonal structure which we refer to as the honeycomb, delineated by the dotted lines in Fig. 2[9]. The electron population of the dots is stable within each cell of the honeycomb and changes when a border between cells is

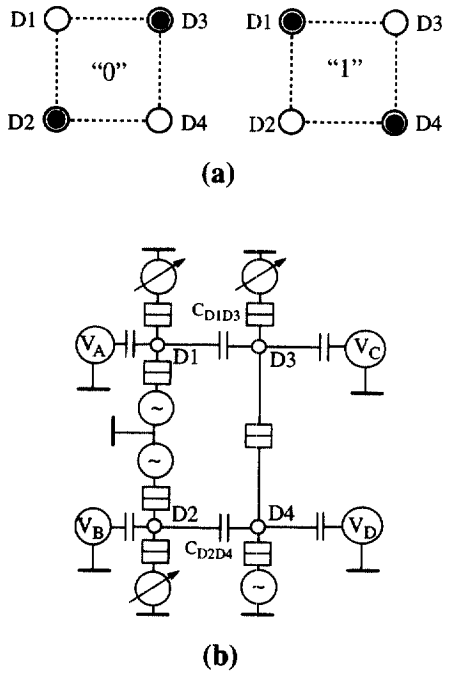

Fig. 1. (a) Basic four-dot QCA cell showing the two possible polarizations. (b) Schematic diagram of the four-dot QCA system.

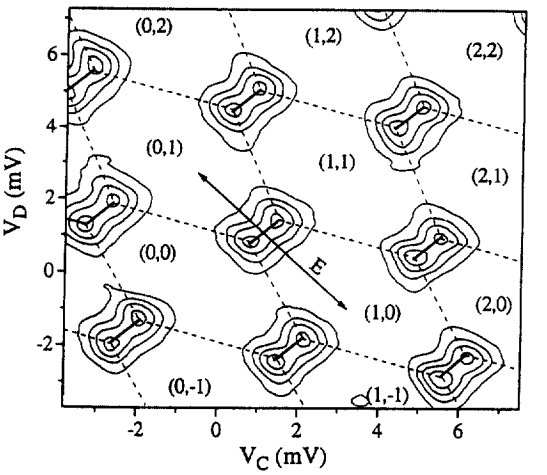

Fig. 2. Contour plot of the measured conductance through the double-dot as a function of V_C and V_D. The excess electron population is noted as (n_3, n_4).

crossed. The excess electron population within each cell can thus be labeled, with the (0, 0) cell centered at $V_C = V_D = 0$ V. A particular setting of V_C and V_D is called the working point and defines a position in the honeycomb. If V_C is swept in the positive direction with V_D fixed, electrons are added one by one to the top dot as the working point moves horizontally through the cells (1, 0) then (2, 0) and so on. If V_D is swept positive, electrons are added to bottom dot as the working point moves vertically through the cells (0, 1) and (0, 2). Most important for QCA operation is motion of the working point in the direction shown by arrow E in Fig. 2. This movement from the (0, 1) to the (1, 0) cell represents the switching of an electron from the bottom dot to the top dot. The goal of QCA operation is to force this transition by the movement of a single electron in the dots D1 and D2.

By applying a positive bias to V_A and a negative bias to V_B, electrons are added one-by-one to D1 and removed from D2, and the electrostatic potential on D1 and D2 changes in response to the applied gate voltages. The potential on D1 increases with the positive voltage V_A, until an abrupt reset which occurs when an electron enters the dot. Thus. the potential of D1 as a function of V_A exhibits a sawtooth pattern. Likewise, the potential on dot D2 is also a sawtooth as a function of V_B. Since the potentials on D1 and D2 act as additional gate voltages for D3 and D4, the honeycomb will shift as electrons switch in D1 and D2, and if the shift is sufficient to move the honeycomb from one side of the working point to the other an electron will switch in the double-dot D3, D4. The switching of an electron will be reflected in the potential of dots D3 and D4, as seen in Fig. 3(a), which plots the experimentally measured potential on D3 as a function of the input voltages $V_A = -V_B$, along with the theoretically calculated potential at a tempera-

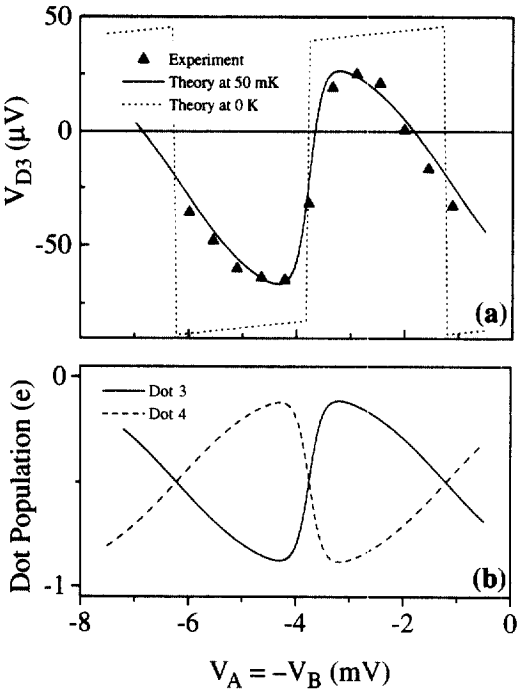

Fig. 3. (a) Measured potential on dot D3 as a function of the differential input $V_A = -V_B$, along with theory at 50 mK and 0 K. (b) Calculated excess electron population for dots D3 and D4 as a function of the differential input.

ture of 50 mK and 0 K. Although at a temperature of 0 K the potential changes are abrupt, the observed potential shows the effects of thermal smearing, and theory at 50 mK gives good agreement with experiment. The heating of the electron system to temperatures above that of the dilution refrigerator is likely due to the applied excitation voltage and noise voltages coupled into the sample by the leads. This effect is commonly seen in measurements of this type[10]. Figure 3(b) plots the theoretical electron population of each of the dots, at 50 mK, showing an 80% polarization switch of the QCA cell, confirming QCA operation. The polarization change can be improved with an increase in the capacitances coupling D1 and D2 to the double dot.

An important requirement for any viable digital logic family is an active element which can provide the voltage gain needed for logic level restoration. This gain is directly related to the noise margin achievable in the logic family: the greater the gain, the greater the noise margin. Our results, shown in Fig. 4, confirm that a QCA cell provides a voltage gain (defined as the ratio of the differential potential $V_{D3}-V_{D4}$ to $V_{D1}-V_{D2}$). Figure 4 plots the theoretical voltage gain of our device at 50 mK, which has a coupling capacitance C_{D1D3} of 100 aF. A voltage gain of 1.1 is obtained, and the gain can

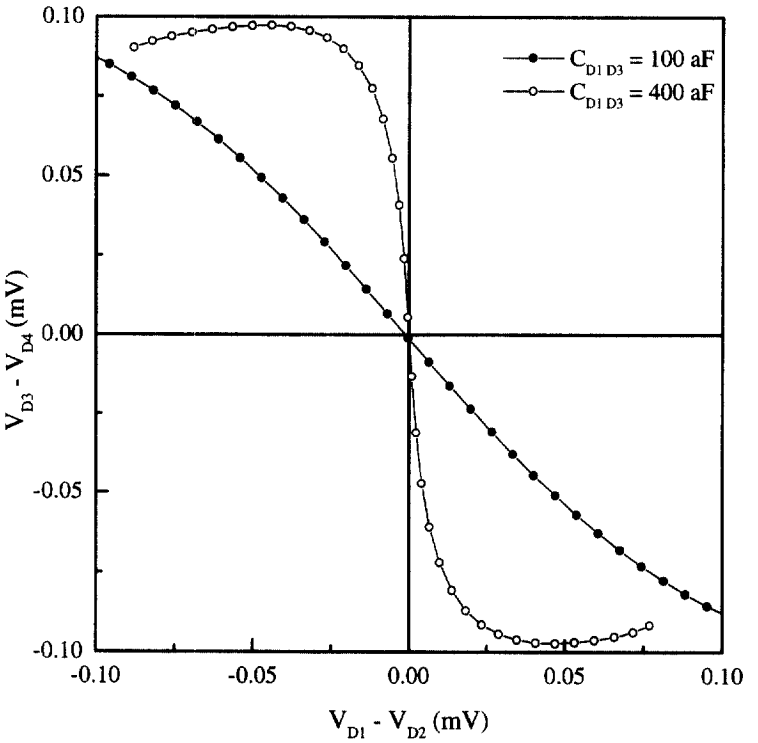

Fig. 4. Voltage transfer characteristic plotting the differential output potential $V_{D3}-V_{D4}$ as a function of the differential input potential $V_{D1}-V_{D2}$.

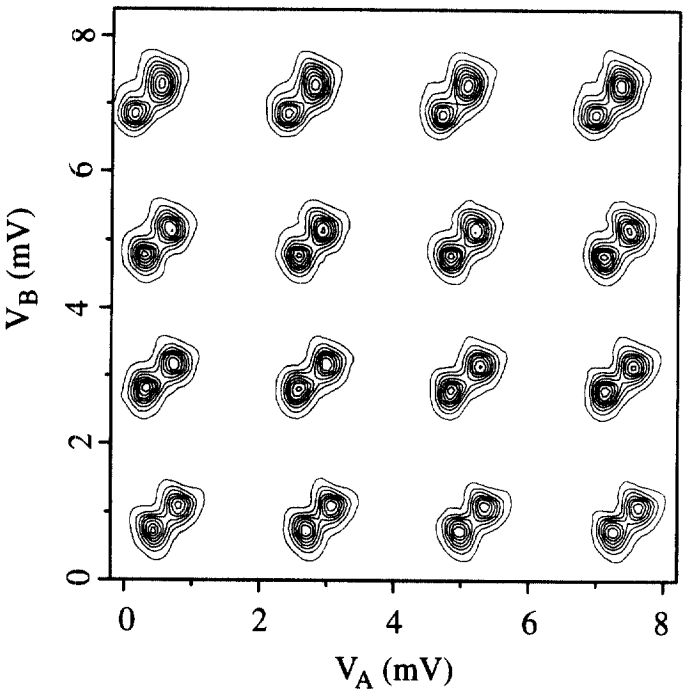

Fig. 5. Contour plot of the measured conductance through the double-dot D1, D2 as a function of V_A and V_B.

be increased to 13.9 by increasing the capacitance value to that of the junction capacitance, 400 aF. This voltage gain shows that quantum devices can be 'active' devices and can provide the logic level restoration needed for digital logic, replacing the traditional active devices such as transistors.

In our latest experiments, improvements have been made to both the measurement techniques and to the device design. In experimental measurements, the effect of parasitic cross-talk capacitance is a well-known problem in gated structures. Each gate not only influences the adjacent dot, but also neighboring dots via these capacitances. In systems with coplanar gates the parasitic capacitance can be as high as 40% of the intended capacitance. In our experiments on QCA systems it is necessary to make large excursions in the gate voltages to thoroughly test the system. This creates serious problems, since the effect from direct charging of a dot due to cross-talk while sweeping a distant gate can overwhelm the relatively small voltage swings due to charge exchange in a double-dot system. To cancel the effects of cross-talk capacitance, we have implemented the following technique. First, as noted earlier, the capacitance from each gate to every dot is determined using the relationship between the capacitance and the period of a Coulomb blockade oscillations. These values are used to determine the correction voltages needed for each gate to cancel the effect of all the other gates. The software controlling the gate biases adds these corrections to the voltages applied to the system under test. Thus, if one gate is scanned the voltages on the other gates are adjusted to cancel the effect on other islands with a net result of charging only the dot adjacent to the gate. It is important to note that the coupling between the dots is unaffected; only the parasitic effects of the gates are eliminated. An example of the honeycomb pattern obtained using this compensation technique is shown in Fig. 5. It is clearly seen that there is no tilt of the honeycomb pattern in the horizontal direction. A small but visible displacement in the vertical direction is caused by the slow variation in the background charge over the several hours required to perform the measurement.

The next set of experiments involve a six dot QCA system, whose simplified schematic is shown in Fig. 6. The design of this system consists of a four-dot QCA cell composed of two double-dots (D1 to D4), where the coupling capacitances C_{D1D3}

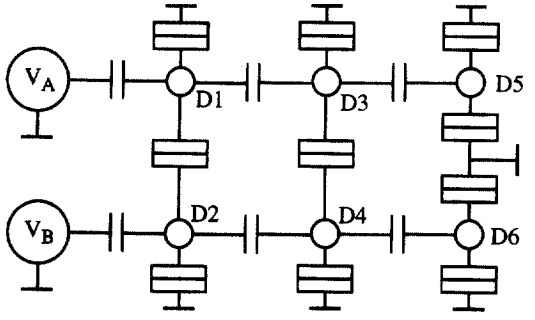

Fig. 6. Simplified schematic of the six-dot QCA system.

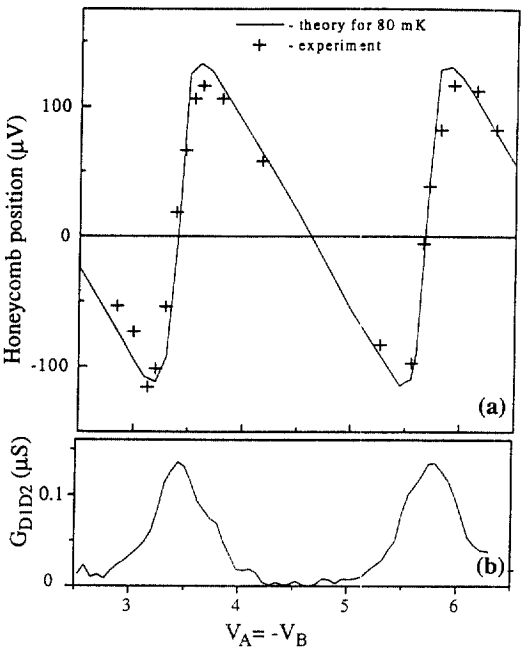

Fig. 7. (a) The position of the honeycomb border of the double-dot D3, D4 as a function of the differential input voltage, along with theory at 80 mK. (b) The conductance through the double-dot D1, D2 as a function of the differential input voltage.

and C_{D2D4} have been increased from the previous design. Two dedicated single dot electrometers, D5 and D6, are connected to the right double dot. As in the previous experiment, we apply a differential input $V_A = -V_B$, and measure the shift in the honeycomb of the double-dot D3, D4 as electrons move from D2 to D1. The honeycomb shift, shown in Fig. 7(a), exhibits a sawtooth characteristic with a maximum shift along the diagonal of 250 μV. Each time the border crosses zero (the working point), an electron switches between the dots D3 and D4. The best fit by theory is obtained at a temperature of 80 mK. Here the cancellation of parasitic capacitances has played an important role, since without compensation the parasitic capacitances would cause a tilt in the sawtooth of Fig. 7(a) which moves the border away from the working point and suppresses QCA operation. Figure 7(b) shows the conductance through the double-dot D1, D2 which exhibit a peak at each reset of the honeycomb border shift. Since the peaks occur when an electron moves from D2 to D1, this confirms that the honeycomb shift is due to single electron switching between D2 and D1.

3. SUMMARY

A device paradigm based on QCA cells offers the opportunity to break away from FET based logic, and to exploit the quantum effects that come with small size. In this new paradigm, logic levels are no longer encoded as voltages but as the position of electrons within a quantum dot cell. QCA cells are scalable to molecular dimensions, and the performance improves as the size shrinks. A QCA cell with molecular dimensions can operate at room temperature. We have demonstrated the first operation of a QCA cell fabricated in aluminum islands with aluminum oxide tunnel junctions. The cell exhibits a bistable distribution of electrons, and the polarization of the cell can be switched by applied bias voltages. The first operation cell showed a voltage gain of 1.8, a value that can be improved dramatically with an optimized design. Preliminary results obtained from an improved six dot system confirm QCA operation, and show the benefit of cancelling the parasitic cross-talk capacitances. It should be emphasized that the cancelling of parasitic capacitances is an important technique in the initial experiments confirming the operation of a QCA cell. In a QCA system it will not be necessary to make large excursions with the input gate biases, and compensation of each dot will not be needed.

Acknowledgements—This work was supported in part by the Defense Advanced Projects Agency, Office of Naval Research, and the National Science Foundation.

REFERENCES

1. Lent, C. S., Tougaw, P. D., Porod, W. and Bernstein, G. H., *Nanotechnology*, 1993, **4**, 49–57.
2. Lent, C. S. and Tougaw, P. D., *Proc. IEEE*, 1997, **85**, 541.
3. Lent, C. S. and Tougaw, P. D., *J. Appl. Phys.*, 1993, **74**, 6227.
4. Tougaw, P. D. and Lent, C. S., *J. Appl. Phys.*, 1994, **75**, 1818.
5. Tougaw, P. D. and Lent, C. S., *J. Appl. Phys.*, 1996, **80**, 4722.
6. Fulton, T. A. and Dolan, G. H., *Phys. Rev. Lett.*, 1987, **59**, 109–112.
7. Orlov, A. O., Amlani, I., Bernstein, G. H., Lent, C. S. and Snider, G. L., *Science*, 1997, **277**, 928.
8. K. K. Likharev, IBM J. Res. Dev., 1988, **32**, 144.
9. Pothier, H. *et al.*, *Physica B*, 1991, **169**, 573.
10. Lafarge, P. *et al.*, *Z. Phys. B*, 1991, **85**, 327.